New two-dimensional porous graphitic carbon nitride nanosheets for highly efficient photocatalytic hydrogen evolution under visible-light irradiation

Journal:	*Catalysis Science & Technology*
Manuscript ID	CY-ART-05-2018-000970.R1
Article Type:	Paper
Date Submitted by the Author:	15-Jun-2018
Complete List of Authors:	Zhang, Longshuai; Institute of Physics, Chinese Academy of Sciences Ding, Ning; Institute of Physics, Chinese Academy of Sciences Wu, Jionghua; Institute of Physics, Chinese Academy of Sciences Iwasaki, Kodai; Tokyo University of Science Lin, Lihua; Fuzhou University, Chemistry Yamaguchi, Yuichi; Tokyo University of Science Shibayama, Yuko; Tokyo University of Science Shi, Jiangjian; Institute of Physics, Chinese Academy of Sciences, Wu, Huijue; Institute of Physics,Chinese Academy of Sciences, Luo, Yanhong; Institute of Physics, Chinese Academy of Sciences, Beijing National Laboratory for Condensed Matter Physics Nakata, Kazuya; Tokyo University of Science, Applied Biological Science Li, Dongmei; Institute of Physics, Chinese Academy of Sciences, Beijing National Laboratory for Condensed Matter Physics Fujishima, Akira; Tokyo University of Science Wang, Xinchen; Fuzhou University, Research Institute of Photocatalysis; Meng, Qingbo; Institute of Physics, Chinese Academy of Sciences,

Journal Name

ARTICLE

New two-dimensional porous graphitic carbon nitride nanosheets for highly efficient photocatalytic hydrogen evolution under visible-light irradiation

Received 00th January 20xx,
Accepted 00th January 20xx

DOI: 10.1039/x0xx00000x

www.rsc.org/

Longshuai Zhang,[ad] Ning Ding,[ad] Jionghua Wu,[ad] Kodai Iwasaki,[b] Lihua Lin,[c] Yuichi Yamaguchi,[b] Yuko Shibayama,[b] Jiangjian Shi,[a] Huijue Wu,[a] Yanhong Luo,[ad] Kazuya Nakata,[b] Dongmei Li,*[ad] Xinchen Wang,[c] Akira Fujishima,*[b], and Qingbo Meng,*[ad]

Aiming at tedious preparation procedures of 2D porous graphitic carbon nitride (2DPCN) nanosheets, a one-step thermal polymerization method based on the supramolecular precursor has been developed. As-prepared 2DPCNs exhibit enlarged specific surface area with rich reaction sites, better crystallinity, stronger visible-light harvesting capability, aligned energy levels and faster charge transfer. A superior photocatalytic hydrogen evolution rate of 220 μmol·h^{-1} under visible-light (λ > 420 nm) irradiation, has been achieved. In the meantime, an apparent quantum yield of 1.3% at 490 nm is also obtained, indicating the 2DPCN possesses green light activity. Our one-step thermal polymerization method based on supramolecular precursor provides a new way to develop C_3N_4 photocatalysts with different morphologies and better photoelectric property.

Introduction

Developing highly efficient photocatalysts has drawn worldwide attention for their potential application in solar energy conversion to chemical energy.[1, 2] Since Wang's pioneering work on graphitic carbon nitride (g-C_3N_4) was reported in 2009, this kind of fascinating metal-free photocatalyst has been attempted in water splitting, pollutant degradation, carbon dioxide reduction and other photocatalytic reactions, due to its adjustable visible-light activity, good stability and low cost.[3-5] However, bulk g-C_3N_4 (BCN) still exhibits rather low photocatalytic activity because of small specific surface area with few photocatalytic active sites, low carrier transfer ability and fast photo-generated carrier recombination.[4] Hence, in order to address these issues, different methodologies including morphological engineering,[6-8] doping,[9-12] or constructing heterostructures,[13-15] have been developed.

As we know, photocatalytic reactions mainly take place on the surface of the photocatalysts, the photocatalytic efficiency is thus closely related to the morphology and microstructure of the materials. 2D materials with extremely small thickness in nanometer even sub-nanometer scales, exhibit attractive advantages for improving the photocatalytic efficiency, such as larger specific surface areas to provide more reactive sites and shorter carrier diffusion lengths to restrain the recombination, in comparison with corresponding bulk materials (i.e. N-doped TiO_2 and $Ba_5Ta_4O_{15}$).[16, 17] g-C_3N_4 is a graphite-like layered polymeric semiconductor, which has strong covalent C-N bonds instead of C-C bonds in each layer and weak Van der Waals force between layers.[18] Obviously, it is desirable to prepare ultrathin 2D g-C_3N_4 materials for higher photocatalytic efficiency.[19, 20] Liu et al. used a direct thermal oxidation "etching" method toward BCN in air to prepare 2 nm-thick g-C_3N_4 nanosheets, which possessed a high specific surface area of 306 $m^2 \cdot g^{-1}$, a larger bandgap by 0.2 eV and a prolonged carrier lifetime.[21] Aiming at low-yield and time-consuming issues, Wu et al. reported a one-step method by using dicyandiamide and NH_4Cl as raw materials, which can release gases to blow dicyandiamide-derived polymers and afford large quantity and high quality g-C_3N_4 nanosheets with an average hydrogen evolution rate of 450 μmol·h^{-1} under the illumination of 300W Xe lamp.[22] Besides, porous structures can also enhance the specific surface area and provide more active sites for various catalytic reactions. Therefore, different porous g-C_3N_4 photocatalysts have also been developed, such as ordered and hollow g-C_3N_4, large pore three dimensional cage-type mesoporous C_3N_4 semiconductors and so on, which exhibited better photocatalytic activity.[6, 23-26]

[a] Key Laboratory for Renewable Energy, Chinese Academy of Sciences (CAS), Beijing Key Laboratory for New Energy Materials and Devices, Beijing National Laboratory for Condensed Matter Physics, Institute of Physics, CAS, Beijing 100190, China
[b] Photocatalysis International Research Center, Research Institute for Science and Technology, Tokyo University of Science, 2641 Yamazaki, Noda, Chiba, 278-0022, Japan
[c] State Key Laboratory of Photocatalysis on Energy and Environment, College of Chemistry, Fuzhou University, Fuzhou 350002, China
[d] School of Physical Sciences, University of Chinese Academy of Sciences, Beijing 100049, China

† Electronic Supplementary Information (ESI) available. See DOI: 10.1039/x0xx00000x

Considering advantages of the above two morphologies, 2D porous g-C_3N_4 (2DPCN) nanosheets are supposed to bring about impressive photocatalytic efficiency. In fact, a few works on this kind of photocatalyst have already been reported.[27, 28] Qu et al. employed solvothermal exfoliation method to obtain atomically thin mesoporous g-C_3N_4 nanomeshes based on freeze-drying assembled dicyandiamide as the precursor.[29] Yang et al. adopted thermal treatment toward BCN under NH_3 atmosphere to afford holey C_3N_4 nanosheets with carbon vacancies, which exhibited an improved photacatalytic performance by about 20 times.[30] Xing et al. prepared macroscopic foam-like holey ultrathin g-C_3N_4 nanosheets by self-modification of polymeric melon units through long-time thermally treating BCN in air.[31] Xu et al. synthesized porous g-C_3N_4 nanosheets by a liquid exfoliation method *via* probe sonication.[32] Chen et al. reported a 2D porous g-C_3N_4 nanosheets/N-doped graphene/layered MoS_2 ternary nanojunction, which exhibited better photodegradation activity of MB.[33] Fan et al. obtained holey structured g-C_3N_4 thin sheets with edge oxygen doping by the BCN oxidization and subsequent exfoliation.[34] However, these synthetic methods usually require tedious procedures, such as long-time solvothermal reaction or thermal exfoliation toward BCN, which especially limit large-scale application of photocatalysts. In addition, as-prepared photocatalysts still suffer from larger bandgaps, disadvantageous to the visible-light utilization.[29-31]

In this regard, a simple one-step thermal polymerization method has been developed for 2DPCN photocatalysts by using a supramolecular precursor, which was obtained by HCl assisted melamine aqueous solution hydrothermal process (Scheme 1). As-prepared 2DPCN shows enlarged specific surface area, better crystallinity, and extended visible-light absorption range. Based on 50 mg photocatalyst, up to 220 $\mu mol \cdot h^{-1}$ of photocatalytic hydrogen evolution rate had been achieved under visible-light (λ > 420 nm) irradiation in the presence of triethanolamine as the sacrifice agent. In the meantime, an apparent quantum yield of 1.3% at 490 nm was also obtained. Further investigation reveals that the remarkable photocatalytic activity of 2DPCN is mainly assigned to its more exposed active sites, and faster interfacial charge transfer/migration due to this kind of 2D porous structure.

Experimental

Materials

Melamine (CP), triethanolamine (AR) and chloroplatinic acid hexahydrate (AR) were purchased from Sinopharm Chemical Reagent Co. Ltd. Hydrochloric acid (37 wt%, AR) was purchased from Xilong Chemical Co. Ltd. All chemicals and reagents were used as received without further purification.

Preparation of 2DPCN

Melamine (2.0 g) was dissolved in 200 mL deionized water, then 2.1 mL HCl was added into the melamine solution while continuously stirring for 30 min. The clear solution was transferred into an autoclave with Teflon liner and heated at 180°C for 10 h. The mixture was filtered to remove the solvent, the precipitate was washed with deionized water and ethanol for several times, and finally dried at 60°C in a vacuum oven overnight. The resultant solid was heated at 650°C for 2 h under a flow of nitrogen with a heating rate of 15°C·min^{-1} to afford the 2DPCN. The yield is ca. 6% based on melamine.

Scheme 1. (a) Preparation process of 2DPCN; (b) Photos of melamine solution, supramolecular precursor and 2DPCN.

Preparation of BCN

For comparison, BCN powder was also synthesized by thermal-polymerization method.[11] In detail, 1 g melamine was directly heated at 650°C for 2 h under a flow of nitrogen with a heating rate of 15°C·min^{-1}. As-prepared BCN was ground to homogeneous powder.

Characterization

XRD patterns of as-prepared samples were collected on a powder X-ray diffractometer (Cu Kα radiation source, D8, Bruker). Morphologies of samples were investigated by scanning electron microscopy (FEI-SEM, XL 30 S-FEG) and transmission electron microscopy (FEI/Tecnai G2 F20 S-TWIN TMP). Specific surface areas and the average porosity distribution of as-prepared samples were obtained by using N_2 adsorption-desorption method on ASAP 2020 apparatus, Micromeritics, which were calculated via Brunauer-Emmett-Teller (BET) method. Fourier transform infrared spectra (FT-IR) were performed on TENSOR 27 spectrometer (Bruker). X-ray photoelectron spectra (XPS) were carried out on ESCALAB 250Xi. Steady-state photoluminescence spectra were carried out under the excitation of 380 nm (Thermo Fisher). UV-visible (UV-Vis) diffuse reflectance spectra were recorded on UV-Vis spectrophotometer (UV-3600, Shimadzu) equipped with an integrating sphere, then converted into absorption spectra by Kubelka-Munk transformation. Electron paramagnetic resonance (EPR) spectra were performed on an ESR spectrometer (JES-FA 200, JEOL) with a modulation frequency of 100 kHz and a microwave power of 1.0 mW. The transient photocurrent property was investigated in a three-electrode cell by using an electrochemical analyser (Model-650A), in which the samples coated on FTO glass act as the working electrode, a Pt wire as the counter electrode, and a Ag/AgCl as the reference electrode. A 300 W Xenon arc lamp light was chosen as a light source while 0.2 M Na_2SO_4 aqueous solution was adopted as the electrolyte at 0.5 V bias. The working electrode was prepared by dropping the catalyst suspension on the FTO glass till its natural drying. The suspension was

prepared by dispersing 5 mg of samples in a mixture of 500 μL H_2O, 500 μL ethanol and 5 μL Nafion solution (5%).

Photocatalytic activity test

Photocatalytic hydrogen production was carried out in a Pyrex top-irradiation reaction cell connected to a closed gas circulation and evacuation system. For each reaction, 50 mg catalyst powder was dispersed in 100 mL aqueous solution containing 10 mL triethanolamine as a sacrificial agent. 3 wt% Pt was loaded on the surface of catalyst by in situ photodeposition of H_2PtCl_6. The reactant solution was evacuated several times to completely remove the air prior to irradiation under a 300W Xe lamp (PLS-SXE300, Trusttech) with a long pass cut-off filter (λ > 420 nm) and a water filter. The temperature of the reactant solution was maintained at 0°C by a flow of cooling liquid during the photocatalytic reaction. The produced gases were analyzed by an on-line gas chromatography equipped with a thermal conductive detector and a 5A molecular sieve column while using argon as the carrier gas. Photocatalytic activities were compared by average hydrogen evolution rate in the first 5h. The apparent quantum yield (AQY) for H_2 evolution was obtained by using a monochromatic LED lamp with the band pass filters of 405, 420, 450, 470, 490, 520 and 578 nm. The irradiation area was controlled as 3×3 cm^2. Depending on the amount of hydrogen gas produced from the photocatalytic reaction in an average of 1h, the AQY was estimated as follows:

$$\mathbf{AQY} = \frac{\mathbf{2 \times\ produced\ hydrogen\ molecule\ numbers}}{\mathbf{incident\ photon\ numbers}} \times \mathbf{100\%}$$

Results and discussion

To g-C_3N_4 photocatalysts, melamine as the starting material is usually adopted in thermal polymerization method, however, high-temperature treatment would lead to a dense g-C_3N_4.[3-5] Recently, a supramolecular precursor from the self-assembly of melamine and cyanuric acid, was reported to enable well keep the morphology after calcination. In addition, the sublimation and/or pyrolysis of melamine and g-C_3N_4 is beneficial to the formation of the porous structure.[11, 12, 23, 35, 36] Here, a one-step thermal polymerization method is developed based on a supramolecular precursor, which was derived from the hydrothermal reaction of melamine in the existence of HCl. The overall synthetic procedure is illustrated in Scheme 1. The structure of the samples are verified by X-ray diffraction (XRD) patterns. As shown in Fig. 1a, there are two obvious XRD diffraction peaks centered at 12.8° and 27.7° for (100) and (002), respectively, similar to those of the BCN. That is, the 2DPCN still possesses typical graphitic carbon nitride characteristics.[3, 4] In addition, a small peak at 21.6° is detected. When melamine is calcinated at a low temperature (under 500°C), this peak can also be detected and the intensity rises with the temperature reduced since low temperatures restrain the polymerization of melon in C_3N_4. Hence, this peak is supposed to be due to the defective condensation of melon structures.[4, 18] However, the peak intensity of 2DPCN is lower

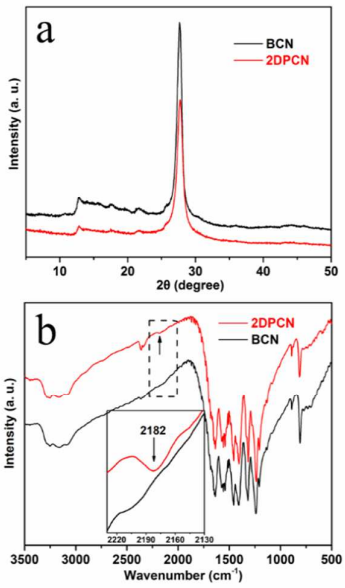

Fig. 1 (a) XRD patterns; (b) FT-IR spectra and partial enlarged detail (inset) of BCN and 2DPCN.

than that of the BCN, indicating less melon structure in the 2DPCN.

Fig. 1b presents typical FT-IR spectra of the obtained samples. Similar FT-IR spectra of the 2DPCN and BCN are observed, also in good agreement with that reported previously.[19] The sharp peak at 810 cm^{-1} is assigned to the typical breathing mode of s-triazine rings. Several strong peaks located between 1700 and 1200 cm^{-1} belong to the skeletal stretching vibration of aromatic C-N heterocycles, while broad peaks in the range 3400-3000 cm^{-1} are ascribed to the stretching vibration of N-H and O-H due to the incomplete polymerization or/and adsorbed water.[23] However, a new peak centered at 2182 cm^{-1} is found in the spectrum of 2DPCN, which is assigned to an asymmetric stretching vibration of C≡N triple bond (Inset in Fig. 1b). The existence of C≡N group in 2DPCN is supposed to increase the electron delocalization and adjust band structures, beneficial for visible-light absorption and photon-generated carrier separation.[37, 38]

The morphologies of supramolecular precursor and 2DPCN are studied by scanning electron microscopy (SEM) and transmission electron microscopy (TEM). The precursor exhibits a micrometer rodlike structure (Fig. 2a). This supramolecular precursor was further calcinated at 650°C for 2h to afford the 2DPCN. As shown in Fig. 2b, the 2DPCN exhibits a uniform nanosheet morphology, and the thickness of 2DPCN nanosheets is estimated to be 50~ 75 nm (Fig. 2c). The high-resolution SEM image in Fig. 2d clearly indicates that this 2D nanosheet is decorated with some pores with the diameters of 30~ 70 nm. In addition, TEM images in Fig. 3a and b further reveal that the 2DPCN has a uniform 2D nanosheet structure, which is decorated with the mesopores with the sizes of 5~ 50 nm, in good agreement with SEM images. For comparison, the BCN derived from the melamine as the raw material, exhibits a bulk material feature (Fig. 3c), which was calcinated by following the same procedure as the 2DPCN. However, to the BCN, no obvious pores are found in the TEM

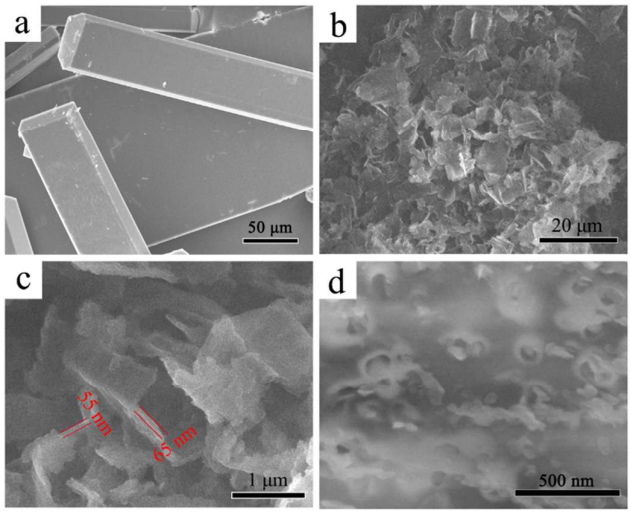

Fig. 2 (a) SEM image of supramolecular precursor; (b)-(d) SEM images of 2DPCN with different enlargement.

image even at high magnification (Fig. 3d). Obviously, the nanosheet morphology and mesopores structure of the 2DPCN can increase the specific surface area. Fig. 3c and f present the selected area electron diffraction (SAED) images of 2DPCN and BCN, respectively. The SAED circular fringes with spot patterns of 2DPCN are marked with corresponding indexes,[39] indicating its growth in a polycrystalline form. However, the SAED of BCN only shows an unsharp amorphous ring. Its thus suggested that, the 2DPCN possesses higher crystallinity degree than BCN. Its known that the higher crystallinity can improve the charge transfer and suppress the charge recombination, which may be beneficial to the photocatalytic activity of 2DPCN.[36]

In order to understand the formation process of the 2DPCN, different calcination temperatures toward the supramolecular precursor were carried out. As shown in Fig. S1a†, the sample calcined at 450°C mainly exhibits a rodlike structure with small holes in the central section of the microrod precursor. When the calcination temperature rises to 550°C, a tubular structure is observed (Fig. S1b†). Further increasing the calcination temperature to 600°C will lead to both nanosheets and tubes, as shown in Fig. S1c†. Based on the above change in the microstructure of as-prepared samples, the formation process of the 2DPCN is suggested. In the calcination process of the rod-structured precursor, a tubular structure is formed at first. With the calcination temperature increasing, more g-C_3N_4 is pyrolyzed until the tube wall is thin enough not to hold the complete tube structure. Finally, the tube would break up into 2D nanosheet. Further investigation reveals that, to precursor solutions with different HCl concentrations (0.075, 0.1 and 0.15 M), similar 2D porous nanosheet structures can also be obtained after calcination, as shown in Fig. S1d-f†. Here, the 2DPCN sample with 0.125 M HCl is taken as example for the further investigation. Furthermore, this one-step thermal polymerization method based on supramolecular precursor, is supposed to be suitable for uniform and large scale preparation of the 2DPCN.

The nitrogen adsorption-desorption isotherms are employed to demonstrate specific surface areas and pore size

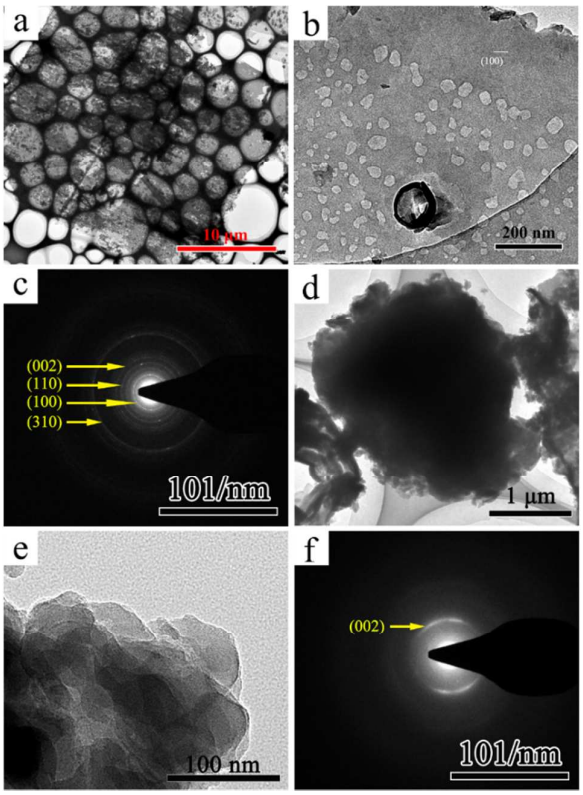

Fig. 3 (a) and (b) TEM images of 2DPCN in different scale bars, (c) the SAED images of 2DPCN; (d) and (e) TEM images of BCN in different scale bars, (f) the SAED images of BCN.

distribution of the 2DPCN and BCN samples. As shown in Fig. 4a, both samples exhibit typical type IV isotherms with an H-type hysteresis loop, suggesting the mesoporous characteristics. And the pore size distribution of the 2DPCN determined by the BJH method, shows a relatively higher content of pores in the whole range with respect to the BCN (see the Inset of Fig. 4a). The specific surface area and pore volume of 2DPCN are 50.2 $m^2 \cdot g^{-1}$ and 0.25 $cm^3 \cdot g^{-1}$, respectively, larger than those of the BCN (14.6 $m^2 \cdot g^{-1}$, 0.13 $cm^3 \cdot g^{-1}$). In this work, the pore formation and pore volume enlargement are mainly assigned to more lateral edges of 2DPCN, which can provide more reduction reaction activity sites for water splitting.[28] As we know, a larger specific surface area can enlarge the contact probability between the photocatalyst and the reactants, which is crucial to the heterogeneous catalysis.[24, 25, 40] Obviously, both the enlarged specific surface area and lateral edges will be beneficial to photocatalytic reactions.

In addition, X-ray photoelectron spectroscopy (XPS) is employed to determine the chemical environment of 2DPCN and BCN. As shown in Fig. S2†, only C, N, and O three elements are investigated in the survey spectra. According to higher-resolution spectra of C 1s, N 1s and Cl 2p in Fig. 4b-c, no obvious changes in binding energies of C1s and N1s are observed for 2DPCN and BCN, and two C1s peaks are located at 288.2 and 284.6 eV, which are related to the sp^2-hybridized carbon in the aromatic ring (N–C=N) and the impurity carbon such as graphitic carbon (C=C), respectively. It is clear that

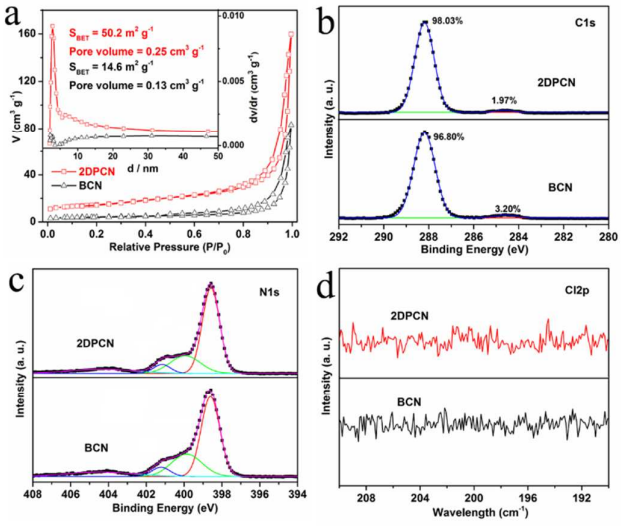

Fig. 4. (a) Nitrogen adsorption-desorption isotherms and BJH pore size distributions (inset). High-resolution XPS spectra of C1s (b), N1s (c) and Cl2p (d) for BCN and 2DPCN.

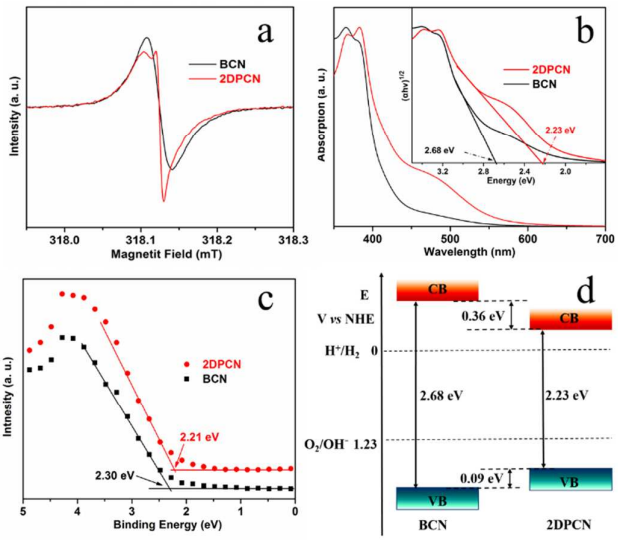

Fig. 5. (a) Room-temperature EPR spectra; (b) UV/Vis light absorption spectra and bandgap energies (inset); (c) XPS valence band spectra and (d) Schematic illustration of the bandgap structure of BCN and 2DPCN (CB= conduction band, VB= valence band).

some carbon impurity in 2DPCN is relatively lower than that in the BCN. The N 1s spectrum can be deconvolved into three peaks centered at 398.6, 399.9 and 401.2 eV (Fig. 4c), which belong to sp^2-hybridized nitrogen in triazine ring (C-N=C), tertiary nitrogen (N-(C)$_3$) and anime group (C-N-H), respectively. And the peak at 404.4 eV is assigned to positive charge localization in heterocycles.[5, 18] Although HCl is involved in the precursor solution, no obvious Cl2p signal is found, indicating the Cl element is not introduced into the 2DPCN, as shown in Fig. 4d. In addition, the C:N ratios of BCN and 2DPCN are estimated by XPS results, that is, the C:N ratio of 2DPCN is 0.72, closer to the theoretical ratio of g-C_3N_4 (0.75) than that of BCN (0.67), suggesting less residual amine groups involved in 2DPCN.[28] Together with the XRD (Fig. 1a) and SAED (Fig. 3c and f) results, the 2DPCN shows a more perfect g-C_3N_4 crystalline structure than that of BCN. This further confirms that our one-step thermal polymerization method has the superiority in preparing high quality 2DPCNs.

Fig. 5a presents electron paramagnetic resonance measurement (EPR) of 2DPCN and BCN. The two samples exhibit a Lorentzian line with *g* value of 2.0031, which is assigned to the unpaired electrons on sp^2-carbon atoms within the π-conjugated aromatic ring.[31] Furthermore, an extra peak at *g*= 2.0049 is found for the 2DPCN, suggesting that the existence of C≡N groups in the 2DPCN can extend the π-conjugated system, in good agreement with the FT-IR spectrum (Fig. 1b).[38, 41] As mentioned above, the C≡N groups can provide a positive effect on photocatalytic reactions.

Electronic band structures of the 2DPCN and BCN are investigated by UV-visible spectra and XPS valence band (VB) spectra. In Fig. 5b, in comparison with BCN, 2DPCN shows an absorption increase in the wavelength range of 420~ 600 nm, primarily due to the multiple reflection of incident light within the porous structure.[28, 29] In the meantime, the corresponding bandgap decreases from 2.68 to 2.23 eV, which is estimated from the Tauc plot (Inset of Fig. 5b). On one hand, higher polymerization degree confirmed by XRD and SAED (Fig. 1a and Fig. 3c and f), is supposed to be beneficial to the bandgap decreased.[11, 42] On the other hand, the existence of C≡N groups in 2DPCN indicates some N vacancies, which can also reduce the bandgap of g-C_3N_4.[37, 38] Although 2DPCN exhibits relatively smaller bandgap, it is still larger than that suitable for splitting water (1.23 eV) even the overpotential involved. Here, by the aid of XPS VB spectra in Fig. 5c, 0.09 eV higher VB edge of the 2DPCN than that of BCN is estimated. Considering the 0.45 eV decrease in the bandgap, the conduction band (CB) of the 2DPCN is thus downshifted by 0.36 eV compared with BCN, as shown in Fig. 5d. On one hand, some decrease in the bandgap of the 2DPCN can lead to visible-light absorption range extended. Meanwhile, the higher VB and lower CB of the 2DPCN can still possess suitable energy levels for water splitting. Generally, the CB of g-C_3N_4 prepared by direct thermal polymerization of melamine, is about -1.1 eV vs. NHE.[4] Obviously, the CB of 2DPCN still has enough reduction ability to release H_2. Therefore, the 2DPCN would be an ideal photocatalyst for visible-light photocatalytic hydrogen evolution.

The photocatalytic hydrogen evolution properties of as-prepared 2DPCNs are tested under visible-light (λ > 420 nm) irradiation by using Pt as the co-catalyst and triethanolamine as the scavenger agent. The influence of different HCl concentrations in the precursor solutions on the photocatalytic hydrogen evolution activity is investigated. As shown in Fig. 6a, all the 2DPCN samples show higher photocatalytic hydrogen evolution rates than BCN, and the highest photocatalytic hydrogen evolution rate is obtained when the HCl concentration is 0.125 M. The effect of heating rates on the photocatalytic hydrogen evolution activity is also investigated (Fig. 6b), and the 15°C·min^{-1} heating rate is found to be the optimal in this work. The highest hydrogen evolution rate of 2DPCN (0.125M) is 220 μmol·h^{-1}, six times higher than that of BCN (34 μmol·h^{-1}), as shown in Fig. 6b. Fig. 6c shows the wavelength dependent apparent quantum yield (AQY) values of the 2DPCN catalyst for H_2 evolution under various

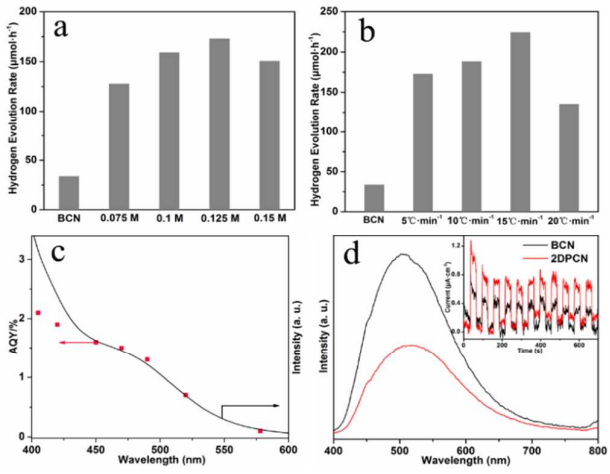

Fig. 6. Photocatalytic hydrogen evolution activity test of the samples under visible-light irradiation (λ > 420 nm). (a) The different HCl concentration of 2DPCNs, (b) the different temperature rate of 2DPCN (0.125M), and (c) wavelength dependent AQY of H_2 evolution over 2DPCN (left axis), UV/vis light absorption spectra of 2DPCN (right axis). (d) Photoluminescence spectra and photocurrent (inset) of BCN and 2DPCN.

monochromatic light irradiation, which variation tendency of AQY curves well corresponds with the UV/Vis light absorption spectrum. The AQY value of 2DPCN is estimated to be about 1.3% at 490 nm. And when irradiated at 520 nm, the AQY value still can reach 0.7%, suggesting that the photocatalytic activity of 2DPCN could be extended to green light. Besides, stronger fluorescence quenching and higher photocurrent response of the 2DPCN (Fig. 6d) are also observed, indicating the charge recombination substantially suppressed and faster photo-generated carrier mobility, both of which are beneficial to highly efficient photocatalytic H_2 evolution. Cycling tests are carried out to explore the photocatalytic stability of the 2DPCN. As shown in Fig. S3a† in ESI, it is found that after four cycle's reactions, the 2DPCN still can keep high-efficiency photocatalytic hydrogen evolution rate. In addition, no obvious difference in XRD and FT-IR spectra of the 2DPCN sample is found before and after the photocatalytic reaction, indicating the 2DPCN exhibits good stability (Fig. S3b and c†).

Conclusions

One-step thermal polymerization method based on a supramolecular precursor has been developed for 2DPCNs. This kind of 2D porous structure is favourable for light harvesting and exhibits rich reaction activity sites. Up to 220 $\mu mol \cdot h^{-1}$ of photocatalytic hydrogen evolution rate has been achieved under visible-light (λ > 420 nm), and an apparent quantum yield of 1.3% at 490 nm has also been obtained, indicating the photocatalytic activity of the 2DPCN can be extended to the green light. Further investigation reveals that the remarkable photocatalytic activity of the 2DPCN is mainly attributed to its extended visible-light absorption range, better crystallinity, aligned energy level and relatively higher specific surface area. More important is that this kind of 2D porous structure can facilitate the interfacial charge transfer/migration. This one-step thermal polymerization method based on supramolecular precursor opens a new way to improve 2DPCN's preparation, structure and photoelectric properties for highly efficient photocatalytic activity.

Acknowledgements

The authors would like to thank the financial support from National Natural Science Foundation of China (Nos. 51627803, 11474333 and 51421002), Sakura Science Program (Japan Science and Technology Agency), and the Knowledge Innovation Program of the Chinese Academy of Sciences.

Notes and references

1 S. S. Chen, T. Takata, K. Domen, *Nat. Rev. Mater.*, 2017, **2**, 17050.
2 Y. Q. Qu, X. F. Duan, *Chem. Soc. Rev.*, 2013, **42**, 2568.
3 X. C. Wang, K. Maeda, A. Thomas, K. Takanabe, G. Xin, J. M. Carlsson, K. Domen, M. Antonietti, *Nat. Mater.*, 2009, **8**, 76.
4 W. J. Ong, L. L. Tan, Y. H. Ng, S. T. Yong, S. P. Cha, *Chem. Rev.*, 2016, **116**, 7159.
5 S. W. Cao, J. X. Low, J. G. Yu, M. Jaroniec, *Adv. Mater.*, 2015, **27**, 2150.
6 K. S. Lakhi, D. H. Park, K. Al-Bahily, W. Cha, B. Viswanathan, J. H. Choyd, A. Vinu, *Chem. Soc. Rev.*, 2017, **46**, 72.
7 J. S. Zhang, F. S. Guo, X. C. Wang, *Adv. Funct. Mater.*, 2013, **23**, 3008.
8 Q. Han, B. Wang, Y. Zhao, C. G. Hu, L. T. Qu, *Angew. Chem. Int. Ed.*, 2015, **54**, 11433.
9 V. W. H. Lau, V. W. Z. Yu, F. Ehrat, T. Botari, I. Moudrakovski, T. Simon, V. Duppel, E. Medina, J. Stolarczyk, J. Feldmann, V. Blum, B. V. Lotsch, *Adv. Energy Mater.*, 2017, **7**, 1602251.
10 L. B. Jiang, X. Z. Yuan, Y. Pan, J. Liang, G. M. Zeng, Z. B. Wu, H. Wang, *Appl. Catal. B: Environ.*, 2017, **217**, 388.
11 L. S. Zhang, N. Ding, M. Hashimoto, K. Iwasaki, N. Chikamori, K. Nakata, Y. Z. Xu, J. J. Shi, H. J. Wu, Y. H. Luo, D. M. Li, A. Fujishima, Q. B. Meng, *Nano Res.*, 2018, **11**, 2295.
12 S. E. Guo, Z. P. Deng, M. X. Li, B. J. Jiang, C. G. Tian, Q. J. Pan, H. G. Fu, *Angew. Chem. Int. Ed.*, 2016, **55**, 1830.
13 W. J. Jiang, W. J. Luo, R. L. Zong, W. Q. Yao, Z. P. Li, Y. F. Zhu, *Small*, 2016, **12**, 4370.
14 Y. Kofuji, Y. Isobe, Y. Shiraishi, H. Sakamoto, S. Tanaka, S. Ichikawa, T. Hirai, *J. Am. Chem. Soc.*, 2016, **138**, 10019.
15 N. Ding, L. S. Zhang, H. Y. Zhang, J. J. Shi, H. J. Wu, Y. H. Luo, D. M. Li, Q. B. Meng, *Catal. Commun.*, 2017, **100**, 173.
16 G. Liu, H. G. Yang, X. W. Wang, L. N. Cheng, J. Pan, G. Q. Lu, H. M. Cheng, *J. Am. Chem. Soc.*, 2009, **131**, 12868.
17 H. Tong, S. X. Ouyang, Y. P. Bi, N. Umezawa, M. Oshikiri, J. H. Ye, *Adv. Mater.*, 2012, **24**, 229.
18 A. Thomas, A. Fischer, F. Goettmann, M. Antonietti, J. O. Muller, R. Schlogl, J. M. Carlsson, *J. Mater. Chem.*, 2008, **18**, 4893.
19 X. H. Song, L. Feng, S. L. Deng, S. Y. Xie, L. S. Zheng, *Adv. Mater. Interfaces*, 2017, **4**, 1700339.
20 J. S. Zhang, Y. Chen, X. C. Wang, *Energy Environ. Sci.*, 2015, **8**, 3092.
21 P. Niu, L. L. Zhang, G. Liu, H. M. Cheng, *Adv. Funct. Mater.*, 2012, **22**, 4763.
22 X. L. Lu, K. Xu, P. Z. Chen, K. C. Jia, S. Liu, C. Z. Wu, *J. Mater. Chem. A*, 2014, **2**, 18924.
23 M. Shalom, S. Inal, C. Fettkenhauer, D. Neher, M. Antonietti, *J. Am. Chem. Soc.*, 2013, **135**, 7118.
24 B. H. Long, Y. Zheng, L. H. Lin, K. A. Alamry, A. M. Asiric, X. C. Wang, *J. Mater. Chem. A*, 2017, **5**, 16179.
25 M. Peer, M. Lusardi, K. F. Jensen, Chem. Mater., 2017, **29**, 1496.

26 S. D. Sun, S. H. Liang, *Nanoscale*, 2017, **9**, 10544.
27 F. Dong, M. Y. Ou, Y. K. Jiang, S. Guo, Z. B. Wu, *Ind. Eng. Chem. Res.*, 2014, **53**, 2318.
28 Y. Y. Kang, Y. Q. Yang, L. C. Yin, X. D. Kang, L. Z. Wang, G. Liu, H. M. Cheng, *Adv. Mater.*, 2016, **28**, 6471.
29 Q. Han, B. Wang, J. Gao, Z. H. Cheng, Y. Zhao, Z. P. Zhang, L. T. Qu, *ACS Nano*, 2016, **10**, 2745.
30 Q. H. Liang, Z. Li, Z. H. Huang, F. Y. Kang, Q. H. Yang, *Adv. Funct. Mater.*, 2015, **25**, 6885.
31 Y. F. Li, R. X. Jin, Y. Xing, J. Q. Li, S. Y. Song, X. C. Liu, M. Li, R. C. Jin, *Adv. Energy Mater.*, 2016, **6**, 1601273.
32 J. D. Hong, S. M. Yin, Y. X. Pan, J. Y. Han, T. H. Zhou, R. Xu, *Nanoscale*, 2014, **6**, 14984.
33 Y. Hou, Z. H. Wen, S. M. Cui, X. R. Guo, J. H. Chen, *Adv. Mater.*, 2013, **25**, 6291.
34 S. N. Guo, Y. Zhu, Y. Y. Yan, Y. L. Min, J. C. Fan, Q. J. Xu, *Appl. Catal. B: Environ.*, 2016, **185**, 315.
35 Y. S. Jun, E. Z. Lee, X. C. Wang, W. H. Hong, G. D. Stucky, A. Thomas, *Adv. Funct. Mater.*, 2013, **23**, 3661.
36 H. H. Ou, L. H. Lin, Y. Zheng, P. J. Yang, Y. X. Fang, X. C. Wang, *Adv. Mater.*, 2017, **29**, 1700008.
37 H. J. Yu, R. Shi, Y. X. Zhao, T. Bian, Y. F. Zhao, C. Zhou, G. I. N. Waterhouse, L. Z. Wu, C. H. Tung, T. R. Zhang, *Adv. Mater.*, 2017, **29**, 1605148.
38 G. G. Liu, G. X. Zhao, W. Zhou, Y. Y. Liu, H. Pang, H. B. Zhang, D. Hao, X. G. Meng, P. Li, T. Kako, J. H. Ye, *Adv. Funct. Mater.*, 2016, **26**, 6822.
39 M. J. Bojdys, J. O. Muller, M. Antonietti, A. Thomas, *Chem. Eur. J.*, 2008, **14**, 8177.
40 X. L. Wang, H. G. Yang, *Appl. Catal. B: Environ.*, 2017, **205**, 624.
41 J. S. Zhang, M. W. Zhang, S. Lin, X. Z. Fu, X. C. Wang, *J. Catal.*, 2014, **310**, 24.
42 L. H. Lin, H. H. Ou, Y. F. Zhang, X. C. Wang, *ACS Catal.*, 2016, **6**, 3921.

One-step thermopolymerization method based on a supramolecular precursor has been developed for preparing 2D porous graphitic carbon nitride.

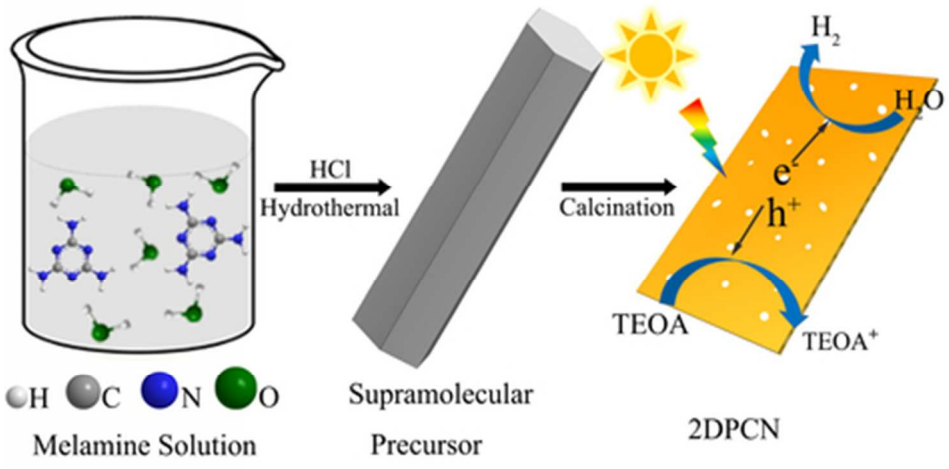

39x19mm (300 x 300 DPI)